Control of Interfacial Instabilities in Thin Polymer Films with the Addition of a Miscible Component

Jamie M. Kropka[†] and Peter F. Green*[,‡]

Department of Chemical Engineering, The University of Texas at Austin, Austin, Texas 78712, and Department of Materials Science and Engineering, Applied Physics, Macromolecular Science and Engineering, The University of Michigan, Ann Arbor, Michigan 48109

Received August 16, 2006; Revised Manuscript Received September 27, 2006

ABSTRACT: We show that while polystyrene (PS) thin films are structurally unstable on oxidized silicon wafers, the addition of as little as a few weight percent tetramethylbisphenol A polycarbonate (TMPC) has a stabilizing effect on the topographical structure of the films. The stabilization is evident from the existence of a threshold TMPC concentration, ϕ_t, and a threshold thickness, h_t, beyond which films do not dewet. The concentration threshold occurs for $\phi_{TMPC} \leq 0.10$. An examination of the effective interface potential, which accounts for short- and long-range intermolecular interactions, indicates that this dewetting inhibition is metastable.

Introduction

A diverse range of applications, from coatings and adhesives to active components in organic electronic devices, rely on the properties and performance of polymer thin films. Both confinement and interactions between the polymer segments and the external interfaces can have a profound influence on the properties exhibited by thin polymer films. Film thickness dependencies of glass transition temperatures (T_g),[1−9] viscosities,[10,11] and phase transitions exhibited by polymer−polymer mixtures and block copolymers[12−15] are all consequences of confinement and interfacial interactions.

In addition to the finite size dependence of physical properties, morphological instabilities also arise in thin polymer films.[16−19] For thin, supported, apolar homopolymer films of thicknesses larger than a few nanometers, morphological destabilization is due to long-range van der Waals forces (though defects and impurities can also be problematic[20,21]).[22−26] The destabilization process begins with the formation of topographical patterns (e.g., spinodal patterns or holes) at the free interface that grow over time. Eventually, the morphological structure evolves to form droplets on the substrate (dewetting). The stability of the system and the mechanism of film breakup can be understood in terms of an effective interface potential or, equivalently, the excess free energy (per unit area) of the film due to the presence of the two interfaces.

Since the performance of most applications relies on uniform films, a number of strategies have been utilized in attempts to stabilize polymer films against breakup. Polymer brush layers, to enable the film to interact with like molecules and reduce unfavorable substrate−film interactions, have been fabricated through the introduction of end-functionalized polymers that can adsorb to the substrate[27−32] or block copolymers with an adsorbing anchor.[33−35] Other strategies include sulfonation and metal complexation of polymer films,[36] surface roughening,[37] and the addition of nanoparticles.[38−41] The retardation of dewetting in these systems is attributed to phenomena that include an increase in film viscosity and/or changes in polymer−substrate interactions. Many of these mechanisms are kinetic in nature, though often the films are stabilized over long time scales that are indicative of an equilibrium phenomenon. We note, however, that none of the above-mentioned studies evaluated the effective interface potential of the system to determine the nature of stabilization.

In this paper, we examine the factors that control the morphological structure of thin film, compatible, mixtures of polystyrene (PS) and tetramethylbisphenol A polycarbonate (TMPC). The majority of studies on polymer−polymer blend thin films have focused on mixtures in the two-phase regime and characterized the interplay between phase separation and dewetting.[42−48] The topographical patterns that develop during both processes are similar, and a careful analysis is necessary to understand their origin. No effects of phase separation are present in our miscible system. Therefore, the topological instabilities that develop are due to long-range van der Waals interactions. We show that while PS thin films are readily destabilized on oxidized silicon wafers, the addition of as little as a few wt % TMPC has a stabilizing effect on the topographical structure of the film. The nature of the stabilization is evaluated in terms of the compositional dependence of both the macroscopic wetting parameters and the effective interface potential, which includes an assessment of both short- and long-range intermolecular interactions.

Experimental Section

Thin films of PS (Pressure Chemical; $M_w = 4$ kg/mol, $M_w/M_n < 1.06$)−TMPC (Bayer; $M_w = 37.9$ kg/mol, $M_w/M_n = 2.75$) mixtures were spin-cast from toluene solution onto clean oxidized silicon wafers. The initial thickness of the polymer film was controlled between 5 and 100 nm by varying solution concentration and spin speed. Silicon (100) wafers (Wafer World, Inc.) with a 2200 nm thermally grown oxide layer were used as substrates. Prior to coating, the wafers were cleaned in an acid solution to remove residual organic contaminants. The acid cleaning consisted of two steps: (1) a 30 min soak in an equal weight mixture of methanol and hydrochloric acid and (2) a 30 min soak in concentrated sulfuric acid. Both acid soaks were followed by rinsing in deionized water and drying by spinning. Immediately before coating, the substrates were rinsed with fresh toluene.

The thickness of the substrate oxide layer and cast films was measured by spectroscopic ellipsometry at room temperature. Films were annealed in a vacuum furnace at $T = 180$ °C, which is sufficiently above the glass transition temperature (T_g)[7] but below the lower critical temperature for mixture phase separation.[49] The

[†] The University of Texas at Austin.
[‡] The University of Michigan.

10.1021/ma061891j CCC: $33.50
Published on Web 11/17/2006

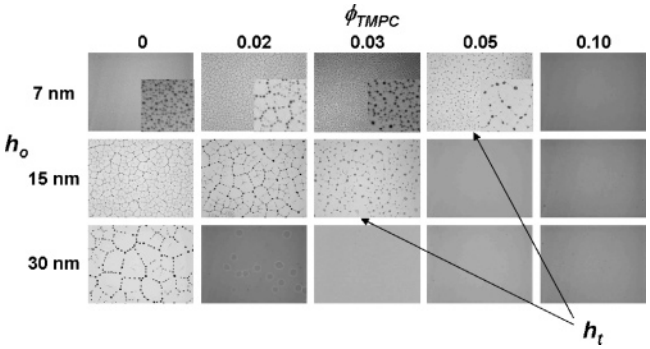

Figure 1. Optical micrographs of PS−TMPC thin film mixtures after annealing. Magnification of all samples is equivalent and shows ∼1 mm in the lateral direction. The 7 nm dewet samples include insets that provide a higher magnification to detail droplet structure. The closely spaced droplets of the 7 nm PS film are the result of spinodal dewetting, whereas the polygonal patterned droplets are the result of hole nucleation and growth. As TMPC concentration increases, droplet shape and patterns become more irregular. In some cases, hole growth was arrested, as in the 30 nm $\phi_{TMPC} = 0.02$ sample. Anneal time varied among individual samples. Films dewet in ≤10 min and were further annealed for up to 2 h to verify no further structure changes. Uniform films were further annealed for ≥16 h with no changes in topography.

samples were annealed until the film broke up to form droplets (if indeed droplets were formed), ≤10 min, and then further annealed and examined until no further structure changes occurred (annealing was continued for up to 2 h for films that dewet and longer than 16 h for films that did not dewet). After annealing, the samples were quenched to room temperature. Surface structure of the substrates, films, and droplets was characterized by optical microscopy and atomic force microscopy (AFM). Optical micrographs were recorded using an Axioskop 2 MAT (Zeiss) with an attached Axiocam MRc5 CCD (Zeiss). All AFM images presented in the results were collected with an Autoprobe CP (Park Scientific) in contact mode with a gold-coated sharpened microlever. The microlevers had a nominal tip radius of 30 nm and a spring constant of 0.05 N/m. Aware of the possibility that contact mode AFM may damage soft polymer structures, we also analyzed selected samples with a Dimension 3100 (Veeco) in intermittent contact. The cantilevers for the Dimension 3100 had a tip radius <10 nm, a nominal spring constant of 42 N/m, and a nominal resonance frequency of 330 kHz. Both AFMs measured equivalent structures over all regions of the substrates, and no regions of damage were noted when reinvestigating samples using intermittent contact. Hence, we only present the originally measured contact mode micrographs. All samples were imaged at room temperature. Images were captured over several locations across the sample to evaluate uniformity across the entire substrate, and scan size was controlled to focus on the pertinent morphological structures.

Results and Discussion

Optical micrographs of PS−TMPC thin film mixtures, after annealing, are shown in Figure 1 and exhibit topographies which range from droplets (due to dewet films) to smooth films, depending on the composition, ϕ_{TMPC}, and initial film thickness, h_0. Stabilization of the films with the addition of TMPC is evident from the following observations. As the TMPC fraction in the film is increased, a composition is reached at which a threshold thickness, h_t, is observed. Beyond h_t, films remain smooth despite annealing at elevated temperatures for longer than 16 h. The threshold film thickness decreases with increasing TMPC concentration until a threshold composition, ϕ_t, is reached, beyond which films do not dewet regardless of thickness. Beyond the thresholds, film uniformity is observed over spatial scales probed by both optical and atomic force microscopy and over time scales 2 orders of magnitude longer than the time it takes for the unstable films to dewet. Determining the underlying factors controlling the observed inhibition of dewetting and whether the stabilization is a kinetic or equilibrium effect is the focus of the following discussion.

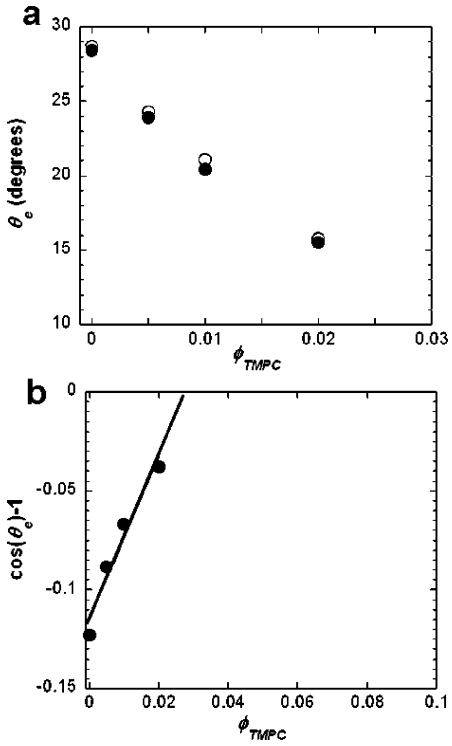

Figure 2. (a) Average contact angle polymer droplets make with the substrate as a function of film composition. Filled points refer to contact line measurements and open points to the spherical cap calculations from droplet diameter and height. The size of the points bound the maximum and minimum contact angle measurements. (b) Linear fit of (cos $\theta_e - 1$) vs concentration data and extrapolation to (cos $\theta_e - 1$) = 0.

Macroscopic Wetting Parameters. When the spreading coefficient for the film is negative, an independent measure of wettability can be obtained from the contact angle, θ_e, that the polymer droplets make with the substrate.[50] The data in Figure 2a, obtained from AFM line profiles of the droplets after the samples had been quenched to room temperature, indicate that the average contact angle decreases with increasing TMPC concentration. To analyze whether the reported contact angles were of equilibrium structures, we compared measurements at the contact line to calculations based on a spherical cap structure and found good agreement, as depicted in Figure 2a. We also found no changes in droplet structure upon further annealing. Further, linear fits of cos θ_e vs contact line curvature (not shown) yielded estimates of the line tension on the order of 10^{-10} J/m, which results in contact angle changes of less than 1° with droplet size over the measured range of droplet radii, ∼1.5−3 μm, to produce the data in Figure 2. The decrease in contact angle with increasing TMPC concentration signifies a decrease in the driving force for dewetting, which is not sufficiently strong to break up films at concentrations of $\phi_{TMPC} \geq 0.10$. In fact, if the concentration dependence of (cos $\theta_e - 1$) is linearly extrapolated to higher concentrations (see Figure 2b), it would reach zero at $\phi_{TMPC} < 0.10$. This suggests an equilibrium nature of the observed dewetting inhibition at $\phi_{TMPC} \geq 0.10$.

The contact angle data enable calculation of the spreading coefficient, S

$$S = \gamma_f(\cos\theta_e - 1) \quad (1)$$

where γ_f is the surface free energy of the film. S is plotted as

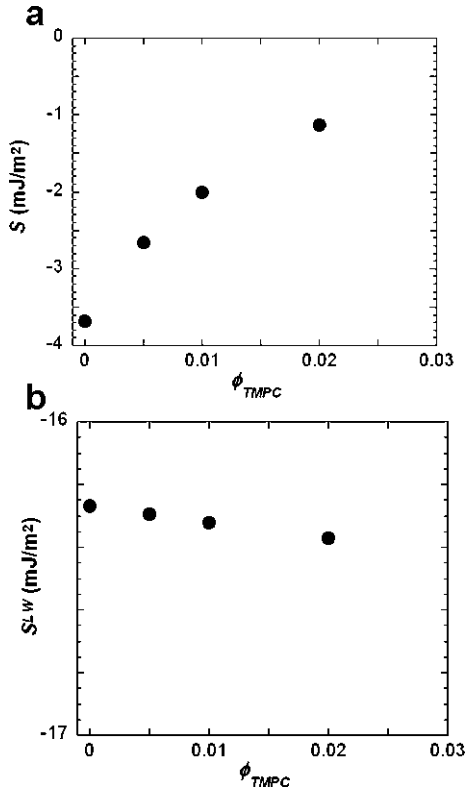

Figure 3. (a) Total spreading coefficient, S, and (b) dispersion component of spreading coefficient, S^{LW}, plotted as a function of film composition. S^{LW} was calculated using the indices of refraction and dielectric constants of materials; $n_{PS} = 1.557$, $n_{TMPC} = 1.586$, $n_{SiOx} = 1.448$, $\epsilon_{PS} = 2.55$, $\epsilon_{TMPC} = 3.17$, $\epsilon_{SiOx} = 3.8$.

a function of film composition in Figure 3a. In all calculations of S, the bulk PS surface energy (29.2 mJ/m^2) is used for γ_f.[51] This approximation is substantiated by the fact that mixture compositions are of $\phi_{TMPC} \leq 0.10$, and PS enriches the free interface of the system.[52] We note that the surface tension of PS has been measured to change when film thickness is decreased below 100 nm,[53] but such changes are sufficiently small as to not alter the conclusions of the following analysis.

To evaluate the origin of TMPC's stabilizing effect, it is instructive to consider both the apolar dispersion contribution, S^{LW}, and the polar contribution, S^p, of the spreading coefficient

$$S = S^{LW} + S^p \tag{2}$$

derived from the apolar and polar components of the interfacial tensions, respectively. S^{LW} and the effective Hamaker constant, A, of the thin film system are related such that[54]

$$S^{LW} = \frac{-A}{12\pi {d_0}^2} \tag{3}$$

where d_0 is the separation distance between materials in van der Waals contact, ~0.15 nm.[55] Equation 3 indicates that knowledge of the Hamaker constant, which can be calculated from refractive indices and dielectric constants of the materials in the layered system,[22] enables the determination of the dispersion component of the spreading coefficient. Using eq 3 and assuming additivity of the refractive indices of the film constituents,[56] S^{LW} is evaluated as a function of film composition as shown in Figure 3b. The polar component of the spreading coefficient may subsequently be deduced as the difference between the total spreading coefficient and the dispersion component via eq 2.

From the data in Figure 3, it is evident that the decrease in contact angle with increasing TMPC content in the film yields an increase in the total spreading coefficient, as ($\cos\theta_e - 1$) approaches zero. On the other hand, the dispersion component of the spreading coefficient decreases with increasing TMPC concentration. Clearly, changes in the dispersion interactions act to destabilize the film as TMPC content is increased and cannot explain the stabilization observed. Therefore, the polar contribution is responsible for the stabilizing effect of TMPC.

We can resolve the increase in S^p by evaluating its contributing components

$$S^p = \gamma_s^p - \gamma_{sf}^p - \gamma_f^p \tag{4}$$

where γ_s^p and γ_f^p are the polar components of the surface free energies of the substrate and film, respectively, and γ_{sf}^p is the polar component of the substrate−film interfacial energy. TMPC enriches the substrate (oxide layer) interface in this system,[52] reflecting favorable TMPC−substrate interactions relative to PS−substrate interactions. Hence, an increase in TMPC coverage of the substrate results in a decrease in γ_{sf}^p. There is no change in γ_s^p with changes in film composition, and negligible change is expected in γ_f^p since we investigated only low TMPC film fractions and PS enriches the free surface of the film.[52] Therefore, it is reasonable to conclude that changes in γ_{sf}^p determine changes in S^p, and the decrease in γ_{sf}^p with increasing TMPC concentration results in the increase in S^p.

Effective Interface Potential. We have shown that a decrease in γ_{sf}^p with increasing TMPC concentration leads to a decrease in the driving force for topographical destabilization of PS−TMPC thin film mixtures and that extrapolation of contact angle measurements suggests an equilibrium nature of the dewetting inhibition at $\phi_{TMPC} \geq 0.10$. However, the onset of the threshold thickness, h_t, beyond which films do not dewet is yet to be explained. To evaluate the stability of the films as a function of film thickness, h, it is convenient to calculate the excess free energy (per unit area) of the film due to the presence of the two interfaces. The excess free energy is the sum of the apolar and polar energies of interaction[22,54,55,57−60] and is often referred to as the effective interface potential of the film, $\Phi(h)$

$$\Phi(h) = \Phi_0^p \exp\left[\frac{d_0 - h}{l}\right] - \frac{A}{12\pi h^2} \tag{5}$$

Here, Φ_0^p is the polar component of the energy of adhesion for interactions at contact ($h = d_0$), l is the decay length of the polar interactions, and A is the effective Hamaker constant. Equation 5 is valid for $h \geq d_0$. For $h < d_0$, the interface potential will increase sharply to infinity due to Born repulsion. Equation 5 may also be written in terms of the macroscopic wetting parameters[54,61]

$$\Phi(h) = S^p \exp\left[\frac{d_0 - h}{l}\right] + S^{LW}\left(\frac{{d_0}^2}{h^2}\right) \tag{6}$$

Therefore, determination of S^p and S^{LW} enables the depiction of the short-range interactions, which decay exponentially with film thickness, and long-range van der Waals interactions, respectively. We use the values of the spreading coefficients as calculated above, and take $l = 0.2$ nm, to plot the effective interface potential for three film compositions in Figure 4.

We first note that our PS potentials are in agreement with those obtained by Seemann et al.[25] for film thicknesses $h >$ ~1 nm. This is to be expected, as the contribution of the

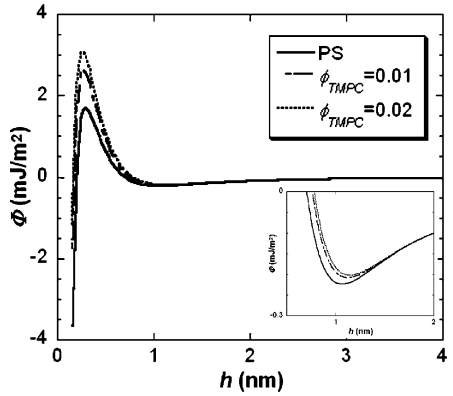

Figure 4. Effective interface potentials for selected film compositions. The plot is of eq 6 and is therefore valid only for $h \geq d_0$. For $h < d_0$, the interface potential will increase sharply to infinity due to Born repulsion. All plotted potentials have a global minimum at d_0, shown as the point at minimum h in the figure. The inset displays the local minima at $h \sim 1$ nm.

dispersion interactions in both analyses is equivalent. However, Seemann[25] calculated the short-range contributions to the potential by fitting the position of a global minimum to $h \sim 1$ nm, $\Phi_{min} \sim -0.25$ mJ/m^2 (defined by a measured thin wetting layer thickness and spreading coefficient, respectively). As mentioned by Muller et al.,[24] such an analysis fails to capture the existence of an additional minimum at short distances that they find through self-consistent-field calculations. Our analysis shows that plots of eq 6 exhibit both minima, which are separated by a barrier in the potential, as in the calculations by Muller.[24] So our analysis provides a method to experimentally describe the contributions of the short-range interactions to the interface potential. Further, the addition of TMPC acts to increase the barrier height and change the contact angle of the macroscopic droplets but has only minor effects on the position of the potential minimum at $h \sim 1$ nm. These effects are similar to those observed by Muller[24] for changes in the contact potential in their calculations. We, reasonably, conclude that TMPC primarily affects the short-range interactions in our system.

The effective interface potential is now examined in light of the nature of the observed dewetting inhibition. We have established that the addition of TMPC primarily affects short-range interactions in the system. This results in the global minimum of the potential residing at a finite thickness even when the value of the potential at contact, $h = d_0$, exceeds the value at $h = \infty$ (i.e., $S > 0$) due to the negative contribution of the long-range van der Waals interactions. This means an autophobic dewetting process, resulting in polymer droplets on a smooth polymer film of thickness h_{min}, corresponding to the location of the minimum in the potential, is thermodynamically predicted when h_{min} is less than the initial film thickness. For our system, h_{min} ($\sim$1 nm) is less than the thinnest films tested ($\sim$7 nm), and therefore autophobic dewetting is anticipated, thermodynamically, for our samples. This signifies that the dewetting inhibition observed with the addition of TMPC is metastable, a conclusion that could not be drawn from analysis of the macroscopic wetting parameters alone.

The existence of h_t and/or ϕ_t could result from the development of an energy barrier to reach the minimum in the effective interface potential or a change in the curvature of the potential with the addition of TMPC, kinetically trapping the film in the uniform state. However, as displayed in Figure 4, changes in the interface potential with TMPC addition are essentially limited to $h < \sim$1 nm and fail to provide insight into the stabilization of thicker films. We therefore question whether the existence of the observed thresholds can be rationalized through analyses of the effective interface potential alone or whether there are additional long-range interactions that are not accounted for in eq 6. Hence, we discuss the possibility of additional stabilization mechanisms below.

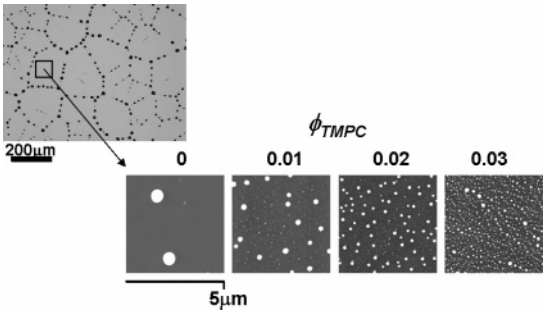

Figure 5. AFM micrographs of PS−TMPC thin film nanostructure after annealing. The optical micrograph in the upper left denotes the region of the samples the AFM micrographs are recorded from. Brighter regions in the AFM micrographs represent larger heights above the substrate. The height range (nm) depicted in the micrographs was set to focus on the pertinent morphological structures and is, from left to right, 40, 25, 15, and 15.

Additional Film Stabilization Mechanisms. The addition of TMPC to the film decreases the dynamics of the system; both the average molecular weight and T_g of the film increase. Changes in dynamics due to an enhancement of film viscosity,[62] however, are less than a factor of 2 and cannot predict an increase in hole nucleation time of 2 orders of magnitude that would be required to explain our stabilization observations.

In other analyses of dewetting retardation, the development of surface heterogeneities has been suggested to play a role in stabilization.[34,37,39,41] In our system, nanodroplets[24,63] are detected by AFM measurements in regions of the substrate between the macroscopic droplets, as shown in Figure 5. From the micrographs in Figure 5, it is clear that the nanodroplets vary in size and spatial distribution with film composition and effectively roughen the substrate surface. As TMPC fraction in the film increases, the nanoscale morphology (nanodroplets) more densely covers the substrate. If the more dense coverage is due to "sticking" of the TMPC chain segments to the substrate and the TMPC chains remain "entangled" with PS neighbors, an increased resistance to dewetting would ensue. Such an effect may, along with the decreasing spreading coefficient, lead to the overall stabilization of the film. Further, with increased initial film thickness, there is more TMPC in the film available to enrich the substrate interface, and the resistance force may increase relative to thinner films. Such a height dependence of the resistance force may play a role in the onset of h_t.

The change in nanodroplet coverage of the substrate is analogous to a change in grafting density of polymer brush layers[32] or nanoparticle substrate coverage with increasing particle concentrations.[39,41] All of these strategies can result in inhibition of dewetting over long time scales that are indicative of a thermodynamic stabilization. However, the exact force that resists the destabilizing van der Waals interactions in these systems remains elusive.

Conclusions

We have demonstrated how morphological analyses of thin film mixtures can be used to deduce changes in the stability of the system with changes in film composition and initial film thickness. The addition of TMPC has a stabilizing effect on the topographical structure of PS films on oxidized silicon

substrates, even at concentrations as low as a few wt %. An analysis of the macroscopic wetting parameters alone suggests a thermodynamic nature of the dewetting inhibition observed in the optical micrographs of Figure 1. However, the change in these parameters is due to changes in the short-range polar interactions between the substrate and polymer film. Although the changes in short-range polar interactions dominate changes in energy at contact, $h = d_0$, these interactions become insignificant at distances $h > \sim 1$ nm from the substrate−film interface and long-range van der Waals interactions determine the film behavior. In our system, changes in these long-range interactions with TMPC addition act to destabilize the film. Therefore, even when interactions at contact are favorable (i.e., $S > 0$), there still exists a minimum in the effective interface potential at $h \sim 1$ nm that defines the thermodynamically stable state of the system: dewet droplets on a thin polymer wetting layer. Additional mechanisms that may stabilize the film against the van der Waals interactions are proposed, but the exact underlying forces remain elusive.

Acknowledgment. This work was funded by the National Science Foundation (DMR 0601890) and the Robert A.Welch Foundation.

References and Notes

(1) Keddie, J. L.; Jones, R. A. L.; Cory, R. A. *Europhys. Lett.* **1994**, *27*, 59−64.
(2) Torres, J. A.; Nealey, P. F.; de Pablo, J. J. *Phys. Rev. Lett.* **2000**, *85*, 3221−3224.
(3) Forrest, J. A.; Dalnoki-Veress, K. *Adv. Colloid Interface Sci.* **2001**, *94*, 167−195.
(4) Long, D.; Lequeux, F. *Eur. Phys. J. E: Soft Matter* **2001**, *4*, 371−387.
(5) McCoy, J. D.; Curro, J. G. *J. Chem. Phys.* **2002**, *116*, 9154−9157.
(6) Pham, J. Q.; Green, P. F. *Macromolecules* **2003**, *36*, 1665−1669.
(7) Pham, J. Q.; Green, P. F. *J. Chem. Phys.* **2002**, *116*, 5801−5806.
(8) Pham, J. Q.; Mitchell, C. A.; Bahr, J. L.; Tour, J. M.; Krishanamoorti, R.; Green, P. F. *J. Polym. Sci., Part B: Polym. Phys.* **2003**, *41*, 3339−3345.
(9) Besancon, B. M.; Soles, C. L.; Green, P. F. *Phys. Rev. Lett.* **2006**, *97*, 057801.
(10) Masson, J.-L.; Green, P. F. *Phys. Rev. E* **2002**, *65*, 031806/031801−031806/031805.
(11) Reiter, G. *Macromolecules* **1994**, *27*, 3046−3052.
(12) Limary, R.; Green, P. F.; Shull, K. R. *Eur. Phys. J. E: Soft Matter* **2002**, *8*, 103−110.
(13) Binder, K. *Adv. Polym. Sci.* **1999**, *138*, 1−89.
(14) Arceo, A.; Green, P. F. *J. Phys. Chem. B* **2005**, *109*, 6958−6962.
(15) Russell, T. P. *Curr. Opin. Colloid Interface Sci.* **1996**, *1*, 107−115.
(16) Reiter, G. *Phys. Rev. Lett.* **1992**, *68*, 75−78.
(17) Reiter, G. *Langmuir* **1993**, *9*, 1344−1351.
(18) Masson, J.-L.; Green, P. F. *Phys. Rev. Lett.* **2002**, *88*, 205504/205501−205504/205504.
(19) Besancon, B. M.; Green, P. F. *Phys. Rev. E* **2004**, *70*, 051808/051801−051808/051808.
(20) Stange, T. G.; Evans, D. F.; Hendrickson, W. A. *Langmuir* **1997**, *13*, 4459−4465.
(21) Jacobs, K.; Herminghaus, S.; Mecke, K. R. *Langmuir* **1998**, *14*, 965−969.
(22) Israelachvili, J. N. *Intermolecular and Surface Forces*; Academic Press: London, 1991.
(23) Reiter, G.; Sharma, A.; Casoli, A.; David, M.-O.; Khanna, R.; Auroy, P. *Langmuir* **1999**, *15*, 2551−2558.
(24) Muller, M.; MacDowell, L. G.; Muller-Buschbaum, P.; Wunnike, O.; Stamm, M. *J. Chem. Phys.* **2001**, *115*, 9960−9969.
(25) Seemann, R.; Herminghaus, S.; Jacobs, K. *Phys. Rev. Lett.* **2001**, *86*, 5534−5537.
(26) Sharma, A.; Khanna, R. *Phys. Rev. Lett.* **1998**, *81*, 3463−3466.
(27) Yerushalmi-Rozen, R.; Klein, J.; Fetters, L. J. *Science (Washington, D.C.)* **1994**, *263*, 793−795.
(28) Yerushalmi-Rozen, R.; Klein, J. *J. Phys.: Condens. Matter* **1997**, *9*, 7753−7765.
(29) Reiter, G.; Auroy, P.; Auvray, L. *Macromolecules* **1996**, *29*, 2150−2157.
(30) Reiter, G.; Schultz, J.; Auroy, P.; Auvray, L. *Europhys. Lett.* **1996**, *33*, 29−34.
(31) Henn, G.; Bucknall, D. G.; Stamm, M.; Vanhoorne, P.; Jerome, R. *Macromolecules* **1996**, *29*, 4305−4313.
(32) Voronov, A.; Shafranska, O. *Langmuir* **2002**, *18*, 4471−4477.
(33) Liu, Y.; Rafailovich, M. H.; Sokolov, J.; Schwarz, S. A.; Zhong, X.; Eisenberg, A.; Kramer, E. J.; Sauer, B. B.; Satija, S. *Phys. Rev. Lett.* **1994**, *73*, 440−443.
(34) Oslanec, R.; Costa, A. C.; Composto, R. C.; Vicek, P. *Macromolecules* **2000**, *33*, 5505−5512.
(35) Costa, A. C.; Composto, R. J.; Vlcek, P. *Macromolecules* **2003**, *36*, 3254−3260.
(36) Feng, Y.; Karim, A.; Weiss, R. A.; Douglas, J. F.; Han, C. C. *Macromolecules* **1998**, *31*, 484−493.
(37) Kerle, T.; Yerushalmi-Rozen, R.; Klein, J. *Europhys. Lett.* **1997**, *38*, 207−212.
(38) Cole, D. H.; Shull, K. R.; Baldo, P.; Rehn, L. *Macromolecules* **1999**, *32*, 771−779.
(39) Barnes, K. A.; Karim, A.; Douglas, J. F.; Nakatani, A. I.; Gruell, H.; Amis, E. J. *Macromolecules* **2000**, *33*, 4177−4185.
(40) Besancon, B. M.; Green, P. F. *Macromolecules* **2005**, *38*, 110−115.
(41) Krishnan, R. S.; Mackay, M. E.; Hawker, C. J.; Van Horn, B. *Langmuir* **2005**, *21*, 5770−5776.
(42) Karim, A.; Slawecki, T. M.; Kumar, S. K.; Douglas, J. F.; Satija, S. K.; Han, C. C.; Russell, T. P.; Liu, Y.; Overney, R.; Sokolov, J.; Rafailovich, M. H. *Macromolecules* **1998**, *31*, 857−862.
(43) Mueller-Buschbaum, P.; O'Neill, S. A.; Affrossman, S.; Stamm, M. *Macromolecules* **1998**, *31*, 5003−5009.
(44) Muller-Buschbaum, P.; Gutmann, J. S.; Stamm, M. *J. Macromol. Sci., Phys.* **1999**, *B38*, 577−592.
(45) Mueller-Buschbaum, P.; Gutmann, J. S.; Stamm, M. *Macromolecules* **2000**, *33*, 4886−4895.
(46) Wang, H.; Composto, R. J. *J. Chem. Phys.* **2000**, *113*, 10386−10397.
(47) Wang, H.; Composto, R. J. *Europhys. Lett.* **2000**, *50*, 622−627.
(48) Mueller-Buschbaum, P.; Bauer, E.; Wunnicke, O.; Stamm, M. *J. Phys.: Condens. Matter* **2005**, *17*, S363−S386.
(49) Kim, E.; Kramer, E. J.; Osby, J. O.; Walsh, D. J. *J. Polym. Sci., Part B: Polym. Phys.* **1995**, *33*, 467−478.
(50) Vitt, E.; Shull, K. R. *Macromolecules* **1995**, *28*, 6349−6353.
(51) Wu, S. *Polymer Interface and Adhesion*; M. Dekker: New York, 1982.
(52) Kim, E.; Krausch, G.; Kramer, E. J.; Osby, J. O. *Macromolecules* **1994**, *27*, 5927−5929.
(53) Ashley, K. M.; Raghavan, D.; Douglas, J. F.; Karim, A. *Langmuir* **2005**, *21*, 9518−9523.
(54) Sharma, A. *Langmuir* **1993**, *9*, 861−869.
(55) Van Oss, C. J.; Chaudhury, M. K.; Good, R. J. *Chem. Rev. (Washington, D.C.)* **1988**, *88*, 927−941.
(56) Seferis, J. C.; Samuels, R. J. *Polym. Eng. Sci.* **1979**, *19*, 975.
(57) Pashley, R. M. *J. Colloid Interface Sci.* **1981**, *83*, 531−546.
(58) Van Oss, C. J. *J. Dispersion Sci. Technol.* **1991**, *12*, 201−219.
(59) Van Oss, C. J.; Chaudhury, M. K.; Good, R. J. *Adv. Colloid Interface Sci.* **1987**, *28*, 35−64.
(60) Ducker, W. A.; Senden, T. J.; Pashley, R. M. *Nature (London)* **1991**, *353*, 239−241.
(61) Sharma, A.; Jameel, A. T. *J. Colloid Interface Sci.* **1993**, *161*, 190−208.
(62) Wisniewsky, C.; Marin, G.; Monge, P. *Eur. Polym. J.* **1984**, *20*, 691−695.
(63) Muller-Buschbaum, P.; Vanhoorne, P.; Scheumann, V.; Stamm, M. *Europhys. Lett.* **1997**, *40*, 655−660.

MA061891J